Martin Etter, Melanie Müller, Michael Hanfland and Robert E. Dinnebier*

Possibilities and limitations of parametric Rietveld refinement on high pressure data: The case study of $LaFeO_3$

Abstract: Parametric Rietveld refinement is a powerful technique to apply directly physical or empirical equations to the refinement of *in situ* powder diffraction data. In order to investigate the possibilities and limitations of parametric Rietveld refinements for high pressure data four competitive crystallographic approaches were used to carry out a full structural investigation of the orthoferrite $LaFeO_3$ (*Pbnm* at ambient conditions) under high pressure up to 47 GPa. Approach A with traditional Rietveld refinement using atomic coordinates, Approach B where the Rietveld refinement was done by using the rigid body method, Approach C where symmetry modes were used and Approach D where the newly developed method of the rotational symmetry mode description for a rigid body was used. For all approaches sequential as well as parametric refinements were carried out, confirming a second order phase transition of $LaFeO_3$ to a higher symmetric phase (space group *Ibmm*) at around 21.1 GPa and an isostructural first order phase transition at around 38 GPa.
Limitations due to non-hydrostatic conditions as well as the possibilities of a direct modeling of phase transitions with parametric Rietveld refinement are discussed in detail.

Keywords: $LaFeO_3$, parametric rietveld refinement, high pressure, phase transition, rotational symmetry modes

*Corresponding Author: **Robert E. Dinnebier,** Max Planck Institute for Solid State Research, Stuttgart, Germany,
e-mail: r.dinnebier@fkf.mpg.de
Martin Etter, Melanie Müller: Max Planck Institute for Solid State Research, Stuttgart, Germany
Michael Hanfland: European Synchrotron Radiation Facility (ESRF), Grenoble, France

1 Introduction

Parametric Rietveld refinement [1, 2] is a powerful technique, which allows the application of physical and/or empirical equations as constraints in the simultaneous treatment of powder diffraction data. In doing so, usually the number of required parameters is reduced, which stabilizes the refinement process and therefore avoids false minima. Additionally even small trends of parameters, which could not be seen before, can be investigated, as the additional stabilization reduces the resulting fluctuations which are expected in a traditional sequential refinement, especially e.g. for small movements of atomic coordinates.

So far parametric Rietveld refinement was successfully applied in for instance the modeling of temperature-dependent structural changes and phase transitions [3], the modeling of kinetics in time-resolved powder diffraction data [4], the modeling of temperature-dependent coupling of strain and order parameters [5] and the modeling of pressure-dependent powder diffractions patterns with different methods [6].

In order to get deeper insight into the applicability and limitations of parametric Rietveld refinement to high pressure powder X-ray diffraction data of perovskites, four competitive crystallographic approaches were used and applied to a typical representative of the class of the rare-earth orthoferrites (space group *Pbnm*) [7–9], namely $LaFeO_3$, which is at ambient conditions structural related to the $GdFeO_3$ aristotype. Approach A with traditional Rietveld refinement of all data, refining fractional atomic coordinates, Approach B where the Rietveld refinement was done by using the method of a rigid body [10, 11] with a deformable body model of the FeO_6 octahedron, Approach C where symmetry modes were used [12–16] and Approach D where the newly developed method of the rotational symmetry mode description for a rigid body was used [17]. All four approaches were carried out with sequential as well as parametric Rietveld refinements, the latter allowing to model the evolution of lattice parameters with equations of state (EoS) [18] up to the hydrostatic limit of the used pressure medium [19] while atomic positions can be modeled with power-law equations derived by Landau theory.

2 Experimental

Using a solid state reaction of a stoichiometric mixture of La_2O_3 and Fe_2O_3, $LaFeO_3$ powder was prepared following the synthesis route according to Peterlin-Neumaier and Steichele [20] and Selbach et al. [21].

For high pressure investigations, the $LaFeO_3$ sample was loaded into a membrane driven diamond-anvil cell (DAC) using a 350 µm diameter culet diamond together with a 4:1 mixture of methanol-ethanol as pressure medium. Diffraction patterns at a wavelength of 0.45584 Å were collected up to pressures of 47 GPa, determining the pressure by the ruby fluorescence method applying the non-linear hydrostatic pressure scale by Mao et al. [22]. A water-cooled Si(111) monochromator with a standard undulator with a 46 mm period was used, in order to achieve highly monochromatic radiation. The beam size of 30×30 µm² was achieved by using slits in horizontal direction, whereas a Pt-coated Si mirror was used for the vertical focusing.

A3 format image plates together with an offline Molecular Dynamics image plate scanner with a pixel size of 100 µm² were used to collect the 2D diffraction patterns. A reduction of the two-dimensional data sets to one-dimensional powder diffraction patterns was done using the program FIT2D [23]. As integration standard a Si reference sample was used.

Sequential as well as parametric Rietveld refinements with the four different approaches were carried out by using the program TOPAS v. 4.2 [24] applying the fundamental parameter approach [25] for peak modeling and Chebyshev polynomials for modeling of the background. The calculations of the symmetry modes (approach C) and the rotational symmetry modes of a rigid body (approach D) were done by using the web-based program ISODISTORT [12].

3 Results

Structural investigations of $LaFeO_3$ were done before by Etter et al. [9], using three different pressure media to identify a second order phase transition of $LaFeO_3$ to a higher symmetric phase (space group *Ibmm*) at around 21.1 GPa and an isostructural first order phase transition at around 38 GPa. In addition, it was shown that the behavior of the lattice parameters can be modeled either with the linearized inverted Murnaghan EoS [9, 26, 27] or with an approach of a linearized inverted Vinet EoS approximation [28]. The modeling with the linearized inverted Murnaghan EoS was later used in the parametric Rietveld refinements of this work.

For all approaches, sequential Rietveld refinements were first carried out, which means that refined parameters of a diffraction pattern at lower pressure were taken as starting parameters for the next pattern at higher pressure. These sequential refinements were then used for a first estimatation on which parameters can be parameterized.

Due to geometric restrictions of the DAC, all Rietveld refinements of the powder X-ray diffraction patterns were limited to a 2θ-range of 5–20.8°. To allow for better comparisons between the different approaches, every diffraction pattern possesses an individual overall isotropic atomic displacement parameter and an individual phenomenological strain parameter which were used in the sequential as well as in the parametric Rietveld refinements. In cases where an anisotropic peak broadening at higher pressure values due to the loss of hydrostatic conditions occurred, symmetry adapted spherical harmonics of low order were individually introduced for these patterns. The zero shift for all diffraction patterns was determined from the first pattern and then fixed throughout all subsequent refinements.

3.1 Approach A: Free Rietveld refinement

The first approach deals with the traditional or free Rietveld refinement, as this gives a first insight into the general behavior of lattice parameters, atomic coordinates, strain, etc. of $LaFeO_3$ with increasing pressure. The traditional Rietveld refinement is also a good indicator, if it makes sense to apply one of the further approaches like symmetry modes or rigid bodies.

As sequential Rietveld refinements of the high pressure synchrotron diffraction patterns of $LaFeO_3$, using the same data, were already carried out by Etter et al. [9], this section focuses on the parameterization of these data sets.

3.1.1 Parametric Rietveld refinement

In the case of the high pressure data of $LaFeO_3$ it is possible to model over the entire pressure range partially the lattice parameters and completely two atomic coordinates with appropriate physical equations. An overview which parameters are parameterized, individually refined or fixed in the sequential and in the parametric refinement is given in Table 1.

Tab. 1: Usage of parameters in traditional Rietveld refinement using the sequential and the parametric approach. The word "refined" in the column of the parametric refinements means individually refined for every diffraction pattern.

	Sequential	Parametric
Background	refined	refined
Lattice parameters *a, b, c*	refined	Murnaghan EoS up to the hydrostatic limit of 9.8 GPa, above fixed
Atomic coordinates:		
La_*z*, Fe_*x*, Fe_*y*, Fe_*z*, O1_*z*	fixed	fixed
La_*x*, O1_*x*, O2_*x*, O2_*y*, O2_*z*	refined	refined
La_*y*, O1_*y*	refined up to 21.1 GPa, above fixed	Power-law equations with common exponent up to the parametrically determined P_{crit}, above automatically fixed
Phenomenological strain parameter	refined	refined
Overall isotropic atomic displacement parameter	refined	refined
Scale factor	refined	refined
Zero shift	fixed	fixed
Spherical Harmonics for anisotropic peak broadening (if required)	refined	refined

The parameterization of the lattice parameters up to the hydrostatic limit can be done by using a linearized inverted Murnaghan EoS [6, 9, 27]:

$$a(P) = a_0 \cdot \left(1 + \frac{K_0' \cdot P}{K_0}\right)^{-\frac{1}{3 \cdot K_0'}} \quad (1)$$

where $a(P)$ is the lattice parameter at a certain pressure P, a_0 is the lattice parameter at ambient conditions, K_0 is the linear modulus and K_0' is its first pressure derivative.

In general, the use of such a linearized and inverted EoS has some advantages in the application of parametric refinements, as in contrast to other EoS, like the Birch-Murnaghan EoS [29] or the Vinet EoS [30], which are normally expressed as P(V) relations, the Murnaghan EoS can be analytically inverted and in doing so it gives direct access to a volume on pressure dependence[1]. Although the volume is not a directly refineable parameter, further linearization can be done, to get the dependence of the lattice parameter on pressure. This linearization is fully valid for cubic materials, whereas it is a reasonable approximation for tetragonal or orthorhombic cases. Considering the main restriction for the use of the Murnaghan EoS, namely, that it is only valid up to a compression of approximately 10% [6, 27], a parameterization can be carried out without loss of refinement quality, as this compression level is first reached at the critical pressure of the second order phase transition, which is far beyond the hydrostatic limit of the used pressure medium. This means that below the hydrostatic limit the Murnaghan EoS will be fully applicable in the parameterization, whereas above, the lattice parameters have either to be individually refined or to be fixed to the values determined by the sequential Rietveld refinement. To ensure a stable refinement, the second alternative was chosen as can be seen in Table 1 and Fig. 1.

Other parameters which can be parametrically modeled by unnormalized power law equations are the lanthanum *y*-coordinate and the *y*-coordinate of O1:

$$La_y(P) = La_y(0) \cdot (P_{crit} - P)^{\beta} + La_{HS} \quad (2)$$

where $La_y(P)$ is the *y*-coordinate value at a certain pressure P, P_{crit} is the critical pressure at which the phase transition takes place, β is the critical exponent and La_{HS} is an additional constant, which accounts for non-zero values of the atomic coordinates in the high symmetry phase. The summation of $La_y(0) \cdot P_{crit}^{\beta}$ and La_{HS} gives the atomic coordinate at ambient conditions and therefore in the low symmetry phase.

In Landau theory commonly a normalized version of Eq. (2) is used, as the normalized version gives a physical amplitude of $La_y(0)$. However, in order to facilitate the computation in the Rietveld refinement software, the unnormalized version will be used, as the amplitude can be analytically converted.

In the parameterization of both coordinates, the exponent β was parameterized as an overall value, as this leads to an additional stabilization in the refinement process. Both atomic coordinates with the sequential as well as with the parametric data points are shown in Fig. 2.

The critical pressure value, which is automatically determined by the parametric Rietveld refinement out of

1 A linearized inverted third order Vinet EoS approximation was recently developed by Etter and Dinnebier [28], which can be used for parameterization in the same way as the above described linearized and inverted Murnaghan EoS.

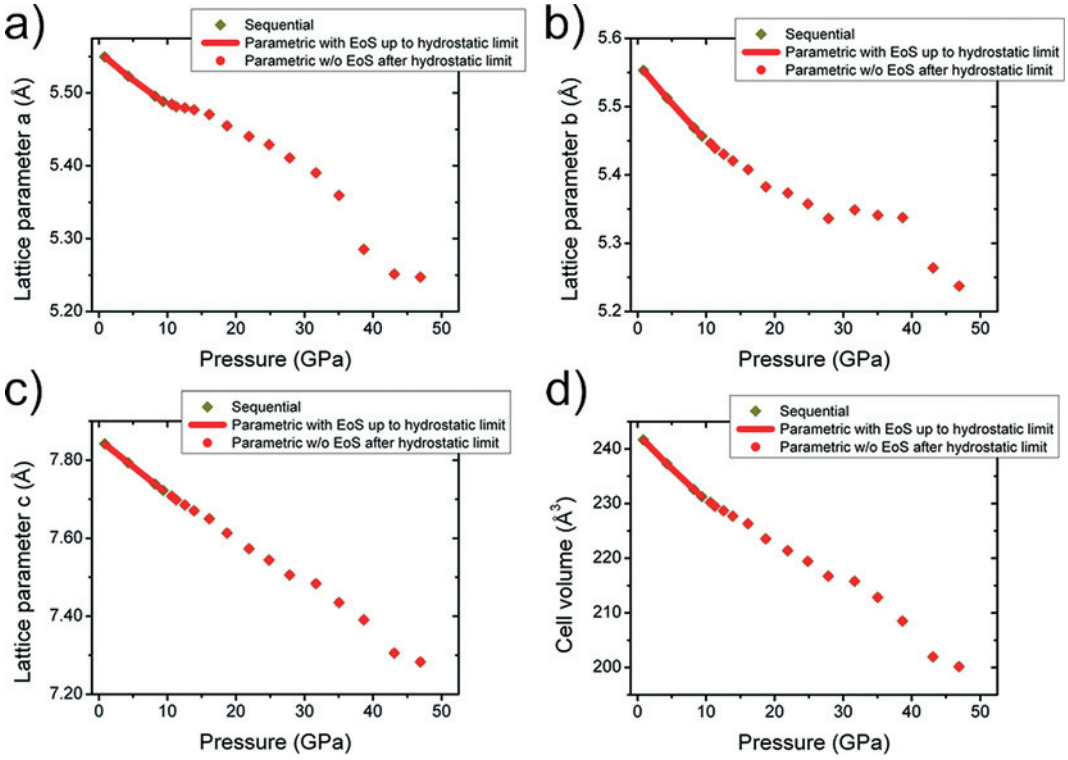

Fig. 1: a)–d). Lattice parameters and cell volume of the sequentially refined high pressure synchrotron diffraction patterns of $LaFeO_3$ with a 4 : 1 mixture of methanol-ethanol as pressure medium. The drop at approximately 38 GPa of 3% in the cell volume, indicating a first order phase transition, is obvious, as already stateted by Etter et al. [9]. The continuous lines and the point symbols are the result of parametric Rietveld refinement.

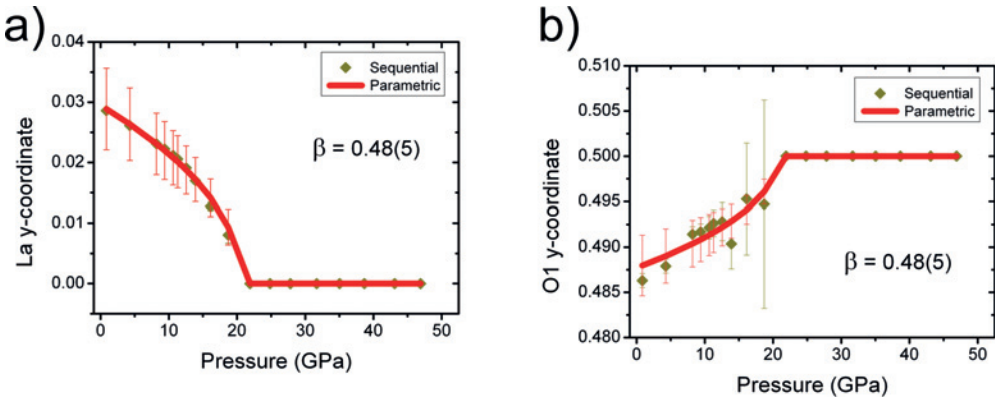

Fig. 2: a) Lanthanum *y*-coordinate of $LaFeO_3$ in dependence on pressure. b) O1 *y*-coordinate of $LaFeO_3$ in dependence on pressure. Both atomic *y*-coordinates indicate a phase transition of second order at approximately 20.6 GPa (21.1 GPa determined by Etter et al. [9]). The continuous lines are the result of the parametric Rietveld refinement.

the equations for the atomic coordinates, is 20.6(10) GPa, which is within one estimated standard deviation in agreement with the value of 21.1(8) GPa, which was determined by Etter et al. [9]. The reason, why both values are not in total agreement is that the value of 21.1 GPa by Etter et al. [9] is determined by using more data points of the lanthanum *y*-coordinate, as they used additional data sets refined from diffraction patterns with other pressure media.

Typically one would expect, that the coordinates *x* and *y* of the oxygen atom O2, which are also part of the phase transition between the space groups *Pbnm* and *Ibmm*, can also be modeled with the above introduced power-law behavior. However, it was not possible to fit these coordinates with appropriate power-laws, as the exponents of these power-laws tend to unphysical values in the present parameterization. For this reason the values of these coordinates were individually refined.

Tab. 2: Linear modulus K_0 and its first pressure derivative as well as the lattice parameters of $LaFeO_3$ at ambient conditions calculated by parametric Rietveld refinement (between 0 and 9.8 GPa) and literature values from Etter et al. [9] who determined the values from another 4:1 methanol-ethanol series, with more data points up to the hydrostatic limit.

Lattice direction	Linear modulus K_0 (GPa)	First pressure derivative K_0'	Linear modulus K_0 (GPa)	First pressure derivative K_0'	Lattice parameter at zero pressure and 300 K (Å)
	Parametric Rietveld refinement		Sequential Rietveld refinement of Etter et al. [9]		
a	215(7)	8.1(11)	209(3)	9.2(7)	5.556(1)
b	150(3)	2.4(5)	142(1)	4.2(3)	5.564(1)
c	186(3)	−0.1(6)	176(1)	1.5(3)	7.86(1)

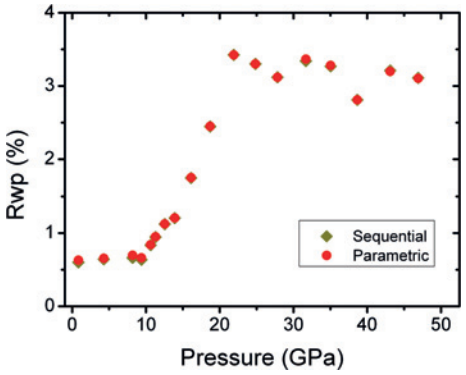

Fig. 3: R_{wp} values of the parametric and of the sequential refinements for $LaFeO_3$ in dependence on pressure. The congruence of the R_{wp} values indicates the correctness of the applied physical constraints.

The results of the parameterized linearized inverted Murnaghan EoS can be found in Table 2. As can be seen from this table, the differences between the parametrically determined values of the linear modulus and its pressure derivative deviate quite much from the values determined by Etter et al. [9], which is owed to the fact, that too few data points are used below the hydrostatic limit to determine the three variables in Table 2.

A suitable method to estimate the quality of a parametric Rietveld refinement is to compare the values of the weighted residuals for both, the sequential as well as the parametric refinement (see Fig. 3). From such plots the validity of the applied physical or empirical constraints can be estimated.

3.2 Approach B: Rigid body refinement

With the use of rigid body models in Rietveld refinement it is in general possible to reduce the number of refined parameters and with this the degrees of freedom which can lead to false minima in the least squares iteration process [10, 11]. In the case of $LaFeO_3$ it is possible to use the method of a rigid body to establish a deformable body for the distorted iron-oxygen octahedra, which can also be called a soft rigid body as the shape of the octahedra and with this the bond-lengths and the bond-angles are changing with increasing pressure. Unfortunately, in the present case, to account for these shape changes the number of parameters to describe that deformable body is identical to those for free Rietveld refinement with traditional atomic coordinates, as there is no common movement of the atoms participating in the octahedra. However, neglecting the disadvantage that there is no reduction in parameters, the usage of such a deformable body model allows studying the internal and external changes (e.g. bond-lengths, bond-angles) of the FeO_6 octahedra.

In Fig. 4 the deformable body with all bond-lengths and angles which are either refined or calculated are shown. A list of parameters, which are parameterized, individually refined or fixed in the sequential as well as in the parametric refinement is given in Table 3.

In the free Rietveld refinement the oxygen atoms O1 and O2 are participating with five degrees of freedom in the construction of the octahedron. These five degrees of freedom can also be found in the deformable body, where

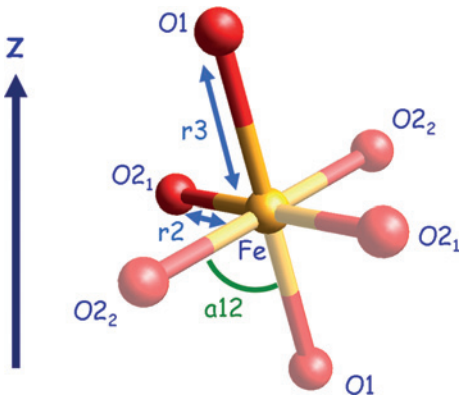

Fig. 4: Deformable body of the FeO_6 octahedron of $LaFeO_3$, connecting the iron atom in the middle and the two oxygen atoms O1 and $O2_1$. The full octahedron which is receveid by symmetry is shown in semi-transparent.

Tab. 3: Usage of parameters in the sequential as well as the parametric Rietveld refinement using the rigid body approach with a deformable body. The word "refined" in the column of the parametric refinements means individually refined for every diffraction pattern.

	Sequential	**Parametric**
Background	refined	refined
Lattice parameters *a*, *b*, *c*	refined	Murnaghan EoS up to the hydrostatic limit of 9.8 GPa, above fixed
Atomic coordinates:		
La_*z*	fixed	fixed
La_*x*	refined	refined
La_*y*	refined up to 21.1 GPa, above fixed	Power-law equation up to the parametrically determined P_{crit}, above automatically fixed
Deformable body coordinates:		
*r*2 (Fe–$O2_1$)	refined	refined
*r*3 (Fe–O1)	calculated by Eq. (3)	Straight line with fixed slope and fixed intercept
a12 (angle $O2_1$–Fe–O1)	refined	refined
rot_a (Rotation around *a*)	refined	fixed
rot_b (Rotation around *b*)	refined	Power-law equation up to theparametrically determined P_{crit}, above individually refined
rot_c (Rotation around *c*)	refined	fixed
Phenomenological strain parameter	refined	refined
Overall isotropic atomic displacement parameter	refined	refined
Scale factor	refined	refined
Zero shift	fixed	fixed
Spherical Harmonics for anisotropic peak broadening (if required)	refined	refined

the bond-length *r*2 (Fe–$O2_1$) and the bond angle a12 (between O1, Fe and $O2_1$/$O2_2$) represent two refineable parameters. The remaining three degrees of freedom are represented by the three rotations around three different axes which are collinear to the crystallographic axes. In contrast to these five refineable parameters, the bond-length *r*3 (Fe–O1) must be calculated by trigonometric considerations. The length of the projection of the bond-length Fe–O1 onto the *c* axis is always *c*/4. Therefore the oxygen atom O1 can move only in the *xy*-plane, which makes it possible to connect the movement with the rotations around the *a*-axis (movement in *y*-direction) and *b*-axis (movement in *x*-direction). From this, one is able to calculate the bond-length *r*3 with the projection and the refined rotation angles rot_a and rot_b by trigonometric considerations as stated by the following equation:

$$r3 = \frac{c}{4} \cdot \cos^{-1}(\mathrm{rot}_a) \cdot \cos^{-1}(\mathrm{rot}_b)\,. \tag{3}$$

3.2.1 Sequential Rietveld refinement

Sequential Rietveld refinements carried out with the deformable body lead to identical results by comparing the R_{wp} values of both, the sequential Approach A and B (see supplementary materials), as the number of degrees of freedom are identical. Investigations of the lattice parameters, atomic coordinates, etc. reveal the same behavior as for approach A, which is expected due to the equality of both approaches.

All bond-lengths and the angle within the deformable body show the expected behavior (see supplementary materials for figures), especially the calculated bond-length *r*3, which is compared to the Fe–O1 bond-length in Fig. 5, calculated from Approach A.

3.2.2 Parametric Rietveld refinement

For the parameterization of Approach B (see also Table 3), the lattice parameters with the linearized inverted Murnaghan EoS up to the hydrostatic limit, the lanthanum *y*-coordinate and the bond-length *r*3 (Fe–O1) can be used, as the bond-length *r*2 (Fe–$O2_1$) and the inner angle *a*12 (O1–Fe–$O2_1$) show no definitive trend suitable for modeling with any kind of equation. Additionally, a parameterization for the rotation angles can be found, if the assumption is made, that the rotations of the octahedron around the *a*- and *b*-axis are constant and that the rotation around the *c*-axis follows the same power-law behavior as for the lanthanum *y*-coordinate (see Fig. 5). With respect to the comparison of the R_{wp} values (see supplementary materials), these assumptions are legitimate, as long as the overall critical exponent β is fixed to a value of $^1/_2$.

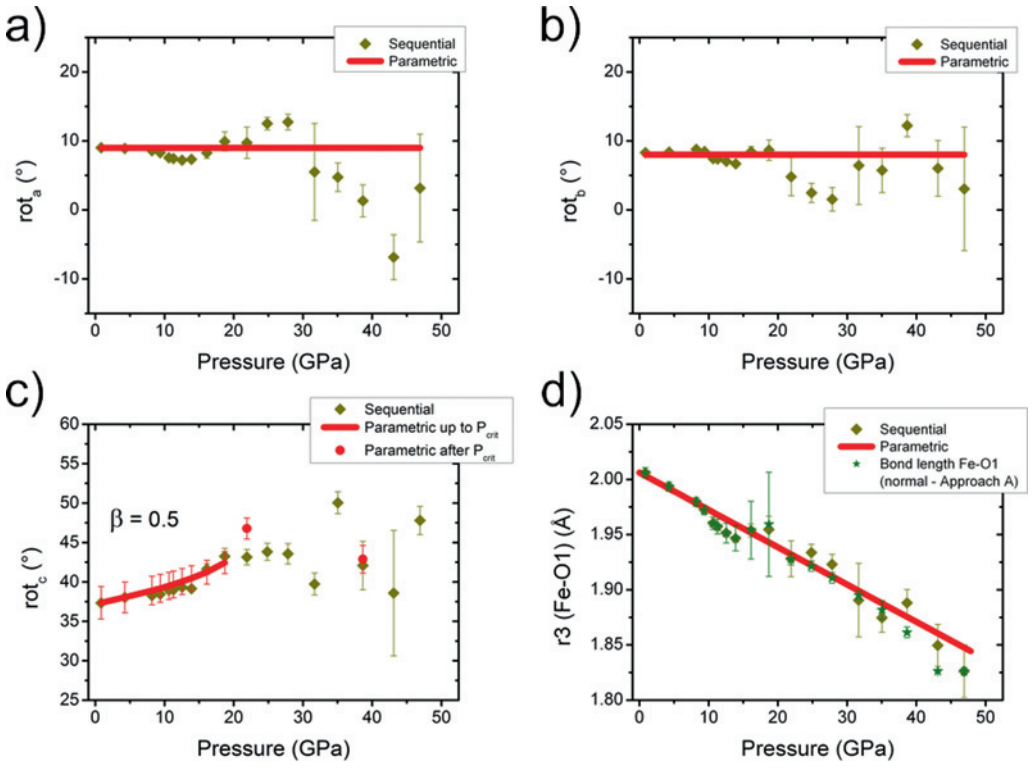

Fig. 5: Rotation angles of the FeO_6 octahedron around the crystallographic axes (a–c) and calculated bond-length *r*3 (Fe–O1) of the FeO_6 deformable body (d) in $LaFeO_3$, compared to the same bond-length wich is calculated out of the coordintes of the free Rietveld refinement. The continuous lines and the point symbols are the result of the parametric Rietveld refinement (for Fig. c) not all point symbols can be seen as they are too wide-spread). The straight line of the *r*3 bond-length shows the parameterized curve with fixed slope and fixed intercept.

A similar obstacle can be found for the parameterization of the bond-length *r*3, where the slope and the intercept needed to be fixed to values obtained from analyzing the sequential refinement (see also Fig. 5). The results of the parameterized lattice parameters and the La *y*-coordinate look similar to Figs. 1 and 2. As expected the determination of the critical pressure by the parametric Rietveld refinement of Approach B faces the same challenges as for Approach A, plus problems in determining adequate rotation angles at higher pressure, leading to a slightly underestimated critical pressure value of 20.8(5) GPa.

3.3 Approach C: Symmetry mode refinement

The symmetry (= distortion) mode approach in crystallography is nowadays a well established method, as it is possible to use a group-subgroup relation to describe a structure with lower symmetry as a distorted parent structure of higher symmetry (e.g. Perez-Mato et al. [13], Iturbe-Zabalo et al. [31], Wang et al. [32], Müller et al. [3]). These structural distortions can be generated by so-called symmetry modes, which can be understood as correlated atomic displacements in real space [13]. Detailed information about the concept of symmetry modes and the usage of irreducible representations of space groups can be found in Campbell et al. [12], Perez-Mato et al. [13], Stokes et al. [14], Hatch and Stokes [15] and Orobengoa et al. [16].

In the case of the $LaFeO_3$ perovskite under high pressure it is possible to establish a group-subgroup relation between the low-symmetric space group *Pbnm* and either the observed higher symmetric space group *Ibmm* or the aristotype space group $Pm\bar{3}m$. Assuming the aristotype structure of $Pm\bar{3}m$, which is a natural choice for perovskites[2] [32], an investigation with ISODISTORT shows that there are two primary order parameters, the R4+ and the M3+ modes, which correspond to tilts of the FeO_6 oc-

2 Depending on the chosen $Pm\bar{3}m$ description, placing the A-cation either on Wyckoff position 1a or 1b the labeling of the mode description will change. The standard description, as chosen above, for such perovskites is with the A-cation on site 1b, B-cation on site 1a and oxygen on site 3d.

Tab. 4: Symmetry modes (denoted with a*) and strain modes (denoted with s*) and their influence on the crystal structure of $LaFeO_3$ using the parental space group $Pm\bar{3}m$. The mode description uses the notation of Miller and Love [33].

Name	Mode description	Influence on
a1	$Pm\bar{3}m$[1/2,1/2,1/2]R5 + (0,a,a) [La1:b]T1u(a)	La *x*
a2	$Pm\bar{3}m$[0,1/2,0]X5 + (0,0,0,0,a,a) [La1:b]T1u(a)	La *y*
a3	$Pm\bar{3}m$[1/2,1/2,1/2]R4 + (0,a,-a)[O1:d]Eu(a)	O1 *x*, O2 *z*
a4	$Pm\bar{3}m$[1/2,1/2,1/2]R5 + (0,a,a)[O1:d]Eu(a)	O1 *x*, O2 *z*
a5	$Pm\bar{3}m$[0,1/2,0]X5 + (0,0,0,0,a,a)[O1:d]Eu(a)	O1 *y*
a6	$Pm\bar{3}m$[1/2,1/2,0]M2 + (a,0,0)[O1:d]A2u(a)	O2 *x*, O2 *y*
a7	$Pm\bar{3}m$[1/2,1/2,0]M3 + (a,0,0)[O1:d]Eu(a)	O2 *x*, O2 *y*
s1	$Pm\bar{3}m$[0,0,0]GM1 + (a)strain(a)	Lattice param.
s2	$Pm\bar{3}m$[0,0,0]GM3 + (a,0)strain(a)	Lattice param.
s3	$Pm\bar{3}m$[0,0,0]GM5 + (a,0,0)strain(a)	Lattice param.

tahedron. In contrast to that, the R5+, X5+ and M2+ modes are secondary modes, which can be attributed to either shifts of the Lanthanum cation or distortions of the FeO_6 octahedron. For the continuous phase transition from *Pbnm* to *Ibmm* only the order parameter M3+ and the secondary modes X5+ and M2+ are needed, as they induce the breaking of the symmetry.

A complete list of all atomic or strain modes and their influence on the atomic coordinates or lattice parameters is shown in Table 4.

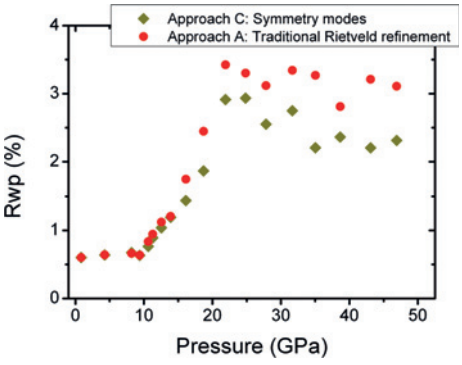

Fig. 6: R_{wp} values of the sequential refinements of Approach A (traditional Rietveld refinement) and Approach C (symmetry modes) for $LaFeO_3$ in dependence on pressure. The lower R_{wp} values of the symmetry mode approach indicate that this approach gives a considerably better stabilization of parameters, especially in the high pressure region.

3.3.1 Sequential Rietveld refinement

In contrast to approach A with the free Rietveld refinement, the symmetry mode approach shows better accuracy for high pressure values, as can be seen in Fig. 6. This behavior of the symmetry mode approach can be explained due to the reduced number of degrees of freedom (see also Table 5), as the M2+ distortion mode (a6) is fixed to zero[3] for all diffraction patterns and therefore leads to a stabilization of the refinement, especially in the high pressure region, where the data quality decreases.

3.3.2 Parametric Rietveld refinement

Due to the fact that in the symmetry mode approach the lattice parameters are calculated by a linear transformation which is performed on linear combinations of strain modes, it is not necessarily possible to simply parameterize the strain modes with a linearized inverted Murnaghan EoS. Therefore the strain modes were neglected for the parameterization and the lattice parameters calculated out of the sequential refinements were used for the parameterization with the linearized inverted Murnaghan EoS (see also Table 5). In contrast to the strain modes, it is possible to parameterize partially the displacement modes as some of them reach zero at the second order phase transition. As the modes a2 and a5 show both a definite trend in the sequential refinements, it is possible to treat the X5+ mode with the same power law behavior as introduced by Eq. (2) for the free Rietveld refinement. Unfortunately this equation cannot be applied to the M3+ tilt mode, as neither the sequential data nor the parametric data show a definite trend of the tilting.

Other modes, not showing definite trends, are not part of the parameterization and are therefore freely refined or fixed (see Table 5, also supplementary materials). For an additional stabilization of the refinement process, the exponent β was parameterized as an overall value for the X5+ mode, which is the identical procedure as in the parameterization of approach A.

3 The amplitude of the M2+ distortion mode is 25 times lower and almost zero in contrast to the M3+ tilting mode.

Tab. 5: Usage of parameters in the sequential as well as the parametric Rietveld refinement using the symmetry mode approach. The word "refined" in the column of the parametric refinements means individually refined for every diffraction pattern.

	Sequential	**Parametric**
Background	refined	refined
Lattice parameters *a*, *b*, *c*	calculated out of three refineable strain modes	Murnaghan EoS up to the hydrostatic limit of 9.8 GPa, above fixed
Atomic coordinates:		
La_*z*, Fe_*x*, Fe_*y*, Fe_*z*, O1_*z*	fixed	fixed
Distortion modes:		
a1 – $Pm\bar{3}m$[1/2,1/2,1/2]R5 + (0,a,a)[La1:b]T1u(a)	refined	refined
a2 – $Pm\bar{3}m$[0,1/2,0]X5 + (0,0,0,0,a,a)[La1:b]T1u(a)	refined up to 21.1 GPa, above fixed	Power-law equation up to the parametrically determined P_{crit}, above automatically fixed
a3 – $Pm\bar{3}m$[1/2,1/2,1/2]R4 + (0,a,-a)[O1:d]Eu(a)	refined	refined
a4 – $Pm\bar{3}m$[1/2,1/2,1/2]R5 + (0,a,a)[O1:d]Eu(a)	refined	refined
a5 – $Pm\bar{3}m$[0,1/2,0]X5 + (0,0,0,0,a,a)[O1:d]Eu(a)	refined up to 21.1 GPa, above fixed	Power-law equation up to the parametrically determined P_{crit}, above automatically fixed
a6 – $Pm\bar{3}m$[1/2,1/2,0]M2 + (a,0,0)[O1:d]A2u(a)	fixed to zero	fixed to zero
a7 – $Pm\bar{3}m$[1/2,1/2,0]M3 + (a,0,0)[O1:d]Eu(a)	refined up to 21.1 GPa, above fixed	refined up to P_{crit}, above fixed
Phenomenological strain parameter	refined	refined
Overall isotropic atomic displacement parameter	refined	refined
Scale factor	refined	refined
Zero shift	fixed	fixed
Spherical Harmonics for anisotropic peak broadening (if required)	refined	refined

From the parametric refinement a critical pressure value of 21.0(12) GPa is obtained, which is in agreement with the correct value which can be reached by fitting the sequential data in approach A.

3.4 Approach D: Refinement with rotational symmetry modes of a rigid body

This new approach of using rotational symmetry modes of a rigid body also called rigid body symmetry modes for Rietveld refinement was developed by Müller et al. [17] and is a natural combination of polyhedral tilts and symmetry modes. More precisely, it combines a rigid body (deformable body) with a vector composed of three rotational symmetry modes, whose values determine the length of the vector which builds the unique rotation axis for the rigid body. Additionally the length of the vector determines the degree of rotation and the values of the modes are used to determine the direction of the vector. With this approach it is possible to rotate the rigid body (deformable body) around any direction, as rotations around the three coordinate axes can be converted into one rotation around one unique axis.

As the three rotational symmetry modes cover already three out of the five possible degrees of freedom of the deformable body (they replace the former rotation angles in approach B, see also Table 7), there are still two degrees of freedom left, which are covered by the bond-length *r*2 (Fe–$O2_1$) and the bond angle a12 (between O1, Fe and $O2_1$/$O2_2$), identical to the assignment in approach B. The bond-length *r*3 (Fe–O1), which was calculated before by two rotation angles must now be calculated by another approach, as the previously used trigonometric considerations can not be any longer used. Therefore a dummy atom X1 with zero occupancy was introduced on the *c*-axis, which has an angle a11[4] between *X*1, Fe and O1, making it possible to use a similar trigonometric consideration as used before in approach B (see also Fig. 7):

$$r3 = \frac{c}{4} \cdot \cos^{-1}(a11) \tag{4}$$

In addition to the rotational symmetry modes and the internal degrees of freedom for the deformable body, two atomic modes for the lanthanum atom and three strain modes for the lattice parameters are needed as can be seen in Tables 6 and 7.

4 The angle a11 can be automatically determined by TOPAS, as the angle between X1, Fe, O1 is a result of the tilting of the deformable body.

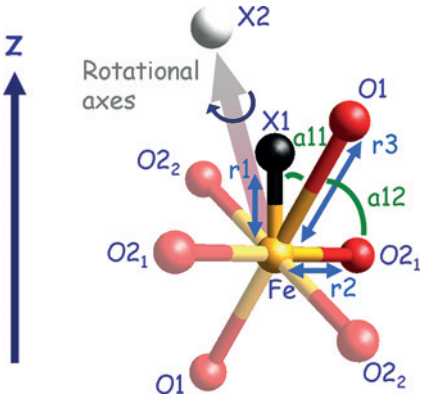

Fig. 7: Deformable body of the FeO_6 octahedron in $LaFeO_3$, connecting the iron atom in the center, a dummy atom X1 (with zero occupancy) and the two oxygen atoms O1 and $O2_1$. The full octahedron which is received by symmetry is shown in semi-transparent. The rotational axis of the deformable body is described by a vector which originates from the center of the rigid body to a dummy atom X2 (with zero occupancy) above. The distance *r*1 ($c/4$) and the angle a11 are calculated by TOPAS.

Tab. 6: Rotational symmetry modes of the FeO_6 deformable body (RB) (denoted with mm*), symmetry modes (denoted with a*) and strain modes (denoted with s*) and their influence on the crystal structure of $LaFeO_3$. The parent space group was for the sake of convenience chosen to be *Ibmm* and the mode description is in the notation of Miller and Love [33].

Name	Mode description	Influence on
a1	*Ibmm*[0,0,0]GM1 + (a)[La1:e]A1(a)	La *x*
a2	*Ibmm*[1,1,1]X4 + (a)[La1:e]B1(a)	La *y*
mm1	*Ibmm*[0,0,0]mGM1 + (a)[Fe1:b]Ag(a)	RB rotation
mm2	*Ibmm*[1,1,1]mX4 + (a)[Fe1:b]Bg_1(a)	RB rotation
mm3	*Ibmm*[1,1,1]mX4 + (a)[Fe1:b]Bg_2(a)	RB rotation
s1	*Ibmm*[0,0,0]GM1 + (a)strain_1(a)	*a*
s2	*Ibmm*[0,0,0]GM1 + (a)strain_2(a)	*b*
s3	*Ibmm*[0,0,0]GM1 + (a)strain_3(a)	*c*

Tab. 7: Usage of parameters in the sequential as well as the parametric Rietveld refinement using the rotational symmetry mode approach. The word "refined" in the column of the parametric refinements means individually refined for every diffraction pattern.

	Sequential	Parametric
Background	refined	refined
Lattice	calculated out of three	Murnaghan EoS up to the hydrostatic limit
parameters *a*, *b*, *c*	refineable strain modes	of 9.8 GPa, above fixed
Atomic coordinates:		
La_*z*, dummy atom X1	fixed	fixed
Distortion modes:		
a1 – *Ibmm*[0,0,0]GM1 + (a)[La1:e]A1(a)	refined	refined
a2 – *Ibmm*[1,1,1]X4 + (a)[La1:e]B1(a)	refined up to 21.1 GPa, above fixed	Power-law equation up to the parametrically determined P_{crit}, above automatically fixed
Rotational modes:		
mm1 – *Ibmm*[0,0,0]mGM1 + (a)[Fe1:b]Ag(a)	refined	fixed
mm2 – *Ibmm*[1,1,1]mX4 + (a)[Fe1:b]Bg_1(a)	refined	Power-law equation up to the parametrically determined P_{crit}, above individually refined
mm3 – *Ibmm*[1,1,1]mX4 + (a)[Fe1:b]Bg_2(a)	refined	fixed
Deformable body coordinates:		
*r*2 (Fe–$O2_1$)	refined	refined
*r*3 (Fe–O1)	calculated by Eq. (4)	Straight line with fixed slope and fixed intercept
a11 (angle O1–Fe–X1)	dependent on rotational modes and automatically determined	dependent on rotational modes and automatically determined
a12 (angle $O2_1$–Fe–O1)	refined	refined
Phenomenological strain parameter	refined	refined
Overall isotropic atomic displacement parameter	refined	refined
Scale factor	refined	refined
Zero shift	fixed	fixed
Spherical Harmonics for anisotropic peak broadening (if required)	refined	refined

3.4.1 Sequential Rietveld refinement

The comparison of the R_{wp} values (see supplementary materials) shows that this new model ensures the same accuracy as approaches A and B. The figures of the strain and atomic modes are not shown as the strain modes for the used parental space group *Ibmm* show the same behavior as the corresponding lattice parameters and the atomic modes are similar to that ones obtained for the symmetry mode approach (see also supplementary materials).

In Fig. 8a) the curves for the rotational symmetry modes are shown, which are used to calculate the rotation angle in Fig. 8b). From these figures it is clear, that with increasing pressure, the error ranges and the fluctuations become quite large, making it a challenge to find a correct parameterization of these modes, as it could be done e.g. for the temperature-dependent example of the double salt $[Mg(H_2O)_6]RbBr_3$ [17]. These fluctuations and large error ranges at high pressures are not exclusively typical for the rotational symmetry mode approach, as they appear also in all other approaches and especially in the free Rietveld refinement, where the atomic coordinates are partially wide-spread.

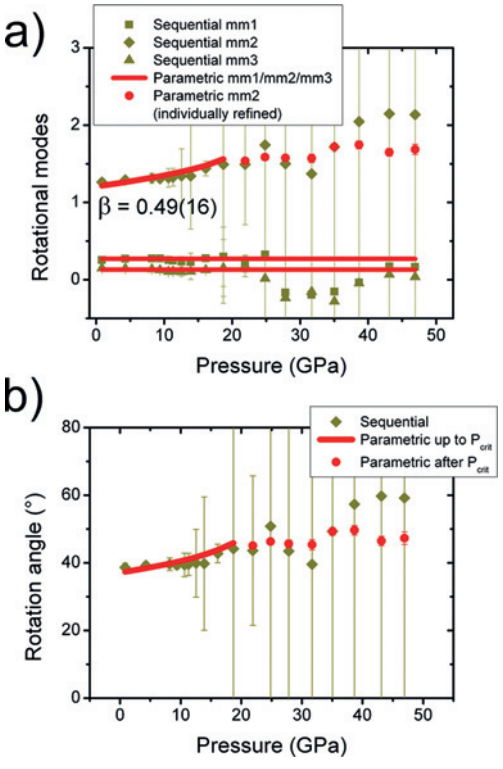

Fig. 8: Rotational symmetry modes mm1–mm3 (a) which are used to calculate the rotation angle (b) of the unique rotation axis. The continuous lines and the point symbols are the result of parametric Rietveld refinement.

3.4.2 Parametric Rietveld refinement

The parameterization which could be performed for the rotational symmetry mode approach is similar as for the symmetry mode and for the deformable body approach. Using the parental space group *Ibmm* instead of $Pm\bar{3}m$, it is possible to calculate each lattice parameter by one individual strain mode, which allows a parameterization of the strain modes with the linearized inverted Murnaghan EoS. Unfortunately, physical values of the linear modulus or of its pressure derivative can not be given, as the transformation from mode space to real space is very complex and should be carried out simultaneously on all the parameters K_0, K_0' and a_0 for a single lattice direction.

As for approach C, the atomic mode which is responsible for the dependence of the lanthanum *y*-coordinate on pressure can also be parameterized (see also Table 7).

In addition to the strain modes and the lanthanum *y*-coordinate all three rotational symmetry modes can be parameterized, if the same assumptions are made as for approach B. In the lower pressure range the modes mm1 and mm3 are approximately constant, whereas the mode mm2 shows a power-law trend up to approximately the critical pressure, until the data quality decreases. Due to this observation, the modes mm1 and mm3 were restricted to fixed values. In contrast to that, the mode mm2 is modeled by the above-mentioned power-law behavior, where the determination of the critical pressure and the critical exponent β is constrained with the determination out of the mode which is responsible for the lanthanum *y*-coordinate. This parameterization led to the same refinement quality as can be seen by the comparison of the R_{wp} values (see supplementary materials).

The obtained critical pressure value for this parameterization is 20.8(39) GPa. This value is very close to the critical pressure which is obtained by free sequential refinement (P_{crit}: 21.1(8) GPa) and identical with that determined by the deformable body refinement (P_{crit}: 20.8(5) GPa).

4 Conclusion

High pressure synchrotron powder X-ray diffraction measurements were carried out for $LaFeO_3$ powder up to pressures of 47 GPa. Sequential as well as parametric Rietveld refinements were performed with four different crystallographic approaches, namely a free traditional Rietveld refinement using atomic coordinates, a Rietveld refinement using the method of rigid bodies, a Rietveld

refinement with symmetry modes and a Rietveld refinement with the new approach of rotational symmetry modes of a rigid body. All four sequential approaches resulted in similar quality of the Rietveld refinements, although the symmetry mode approach showed better refinement results, especially for higher pressure values, as the number of degrees of freedom could be reduced due to the fixation of one symmetry mode. This led to an additional stabilization of the sequential refinement in contrast to the other three approaches, where the numbers of degrees of freedom could not be reduced.

The parametric treatment of all approaches showed that the critical pressure can be satisfactory modeled by a power-law equation, especially for the symmetry mode approach and still sufficient for both deformable body approaches. For the normal symmetry mode approach, the reduced degrees of freedom and the parametric modeling of the X5+ mode led to an almost identical critical pressure value compared to the value determined by Etter et al. [9]. Also for the approach of rotational symmetry modes of a deformable body and the approach of a deformable body using the method of rigid bodies, a conformable critical pressure value could be determined, although some assumptions for the parameterization must be made concerning either rotation angles or rotational symmetry modes. In contrast to these three approaches, the parameterization of the traditional Rietveld refinement approach led to the most underestimated determination of the critical pressure.

The parametric treatment of the lattice parameters up to the hydrostatic limit with linearized and inverted Murnaghan EoS led for all approaches to under- or overestimated values for the bulk modulus and its pressure derivative compared to the values determined by Etter et al. [9], which is due to an insufficient number of data points in that region. Nevertheless they can be used in the parameterization as they led to a further stabilization of the refinement.

In general, approaches using the rigid body method with a deformable body are preferable, as the introduction of a rigid body, partial rigid body or deformable body leads to a reduction of the number of degrees of freedom. These approaches also include the possibility to directly investigate the movement of a group of atoms, especially the metal-oxygen groups in perovskites and therefore the tilting and distortion behavior of these octahedra. This can exclusively be seen in the parametric refinement of approach D, where the movement of the deformable body could be constrained with the movement of the lanthanum *y*-coordinate to determine a common critical pressure and common critical exponent.

Therefore, the symmetry mode approach and the approach of rotational symmetry modes of a rigid body seem to be the most suitable approaches for the investigation of perovskites under high pressure, as they show the largest potential to reduce the number of degrees of freedom, which normally leads to a more stable refinement. This is in particular true in combination with parametric Rietveld refinement, which intrinsically leads to an additional stabilization and therefore more reliable results.

References

[1] Rietveld, H. M.: A Profile Refinement Method for Nuclear and Magnetic Structures. Journal of Applied Crystallography **2** (1969) 65–71.
[2] Stinton, G. W.; Evans, J. S. O.: Parametric Rietveld refinement. Journal of Applied Crystallography **40** (2000) 87–95.
[3] Müller, M.; Dinnebier, R. E.; Schorr, S.: A case study of parameterized Rietveld refinement: The structural phase transition of $CuInSe_2$. Zeitschrift für Kristallographie **226** (2011) 956–962.
[4] Müller, M.; Dinnebier, R. E.; Jansen, M.; Wiedemann, S.; Plüg, C.: Kinetic analysis of the phase transformation form α- to β-copper phthalocyanine: A case study for sequential and parametric Rietveld refinements. Powder Diffraction **24** (2009) 191–199.
[5] Magdysyuk, O. V.; Müller, M.; Dinnebier, R. E.; Lipp, C.; Schleid, T.: Parameterization of the coupling between strain and order parameter for $LuF[SeO_3]$. Journal of Applied Crystallography (accepted).
[6] Halasz, I.; Dinnebier, R. E.; Angel, R.: Parametric Rietveld refinement for the evolution of powder diffraction patterns collected as a function of pressure. Journal of Applied Crystallography **43** (2010) 504–510.
[7] Geller, S.; Wood, E. A.: Crystallographic Studies of Perovskite-Like Compound I. Rare-Earth Orthoferrites and $YFeO_3$, $YCrO_3$, $YAlO_3$. Acta Crystallographica **9** (1956) 563–568.
[8] Selbach, S. M.; Tolchard, J. R.; Fossdal, A.; Grande, T.: Nonlinear thermal evolution of the crystal structure and phase transitions of $LaFeO_3$ investigated by high temperature X-ray diffraction. Journal of Solid State Chemistry **196** (2012) 249–254.
[9] Etter, M.; Müller, M.; Hanfland, M.; Dinnebier, R. E.: High pressure phase transitions in the rare-earth orthoferrite $LaFeO_3$. Submitted to Acta Crystallographica B.
[10] Dinnebier, R. E.: Rigid bodies in powder diffraction. A practical guide. Powder Diffraction **14** (1999) 84–92.
[11] Dinnebier, R. E.; Billinge, S. J. L.: Powder Diffraction – Theory and Practice, Royal Society of Chemistry Publishing, Cambridge (UK) 2008.
[12] Campbell, B. J.; Stokes, H. T.; Tanner, D. E.; Hatch, D. M.: ISODISPLACE: a web-based tool for exploring structural distortions. Journal of Applied Crystallography **39** (2006) 607–614.
[13] Perez-Mato, J. M.; Orobengoa, D.; Aroyo, M. I.: Mode crystallography of distorted structures. Acta Crystallographica A**66** (2010) 558–590.
[14] Stokes, H. T.; Hatch, D. M.; Wells, J. D.: Group-theoretical methods for obtaining distortions in crystals: Applications to vi-

brational modes and phase transitions. Physical Review B**43** (1995) 11010–11018.
[15] Hatch, D. M.; Stokes, H. T.: Complete listing of order parameters for a crystalline phase transition: A solution to the generalized inverse Landau problem. Physical Review B**65** (2001) 014113-1-4.
[16] Orobengoa, D.; Capillas, C.; Aroyo, M. I.; Perez-Mato, J. M.: AMPLIMODES: symmetry-mode analysis on the Bilbao Crystallographic Server. Journal of Applied Crystallography **42** (2009) 820–833.
[17] Müller, M.; Dinnebier, R. E.; Dippel, A.-C.; Stokes, H. T.; Campbell, B. J.: A symmetry-mode description of rigid-body-rotations in crystalline solids: a case study of $Mg[H_2O]_6RbBr_3$. Journal of Applied Crystallography (accepted).
[18] Angel, R. J.: Reviews in Mineralogy and Geochemistry, Vol. **41**, High-Pressure and High-Temperature Crystal Chemistry (2000) 35–60.
[19] Angel, R. J.; Bujak. M.; Zhao, J.; Gatta, G. D.; Jacobsen, S. D.: Effective hydrostatic limits of pressure media for high-pressure crystallographic studies. Journal of Applied Crystallography **40** (2007) 26–32.
[20] Peterlin-Neumaier, T.; Steichele, E.: Antiferromagnetic structure of $LaFeO_3$ from high resolution TOF neutron diffraction. Journal of Magnetism, and Magnetic Materials **59** (1986) 351–356.
[21] Selbach, S. M.; Tolchard, J. R.; Fossdal, A.; Grande, T.: Nonlinear thermal evolution of the crystal structure and phase transitions of $LaFeO_3$ investigated by high temperature X-ray diffraction. Journal of Solid State Chemistry **196** (2012) 249–254.
[22] Mao, H. K.; Xu, J.; Bell, P. M.: Calibration of the Ruby Pressure Gauge to 800 kbar under Quasi-Hydrostatic Conditions. Journal of Geophysical Research **91** (1986) 4673–4676.
[23] Hammersley, A. P.; Svensson, S. O.; Hanfland, M.; Fitch, A. N.; Hausermann, D.: Two-Dimensional Detector Software: From Real Detector to Idealised Image of Two-Theta Scan. High Pressure Research **14** (1996) 235–248.
[24] TOPAS Version 4.2, Bruker-AXS, Karlsruhe, Germany.
[25] Cheary, R. W.; Coelho, A. A.: A fundamental parameters approach to X-ray line-profile fitting. Journal of Applied Crystallography **25** (1992) 109–121.
[26] Murnaghan, F. D.: The Compressibility of Media under Extreme Pressures. Proc. Natl. Acad. Sci USA **30** (1944) 244–247.
[27] Angel, R. J.: Reviews in Mineralogy and Geochemistry, Vol. **39**, Transformation Processes in Minerals (2000) 85–104.
[28] Etter, M.; Dinnebier, R. E.: Direct parameterization of the volume on pressure dependence by using an inverted approximative Vinet equation of state. Journal of Applied Crystallography **47** (2014) 384–390.
[29] Jeanloz, R.: Universal equation of state, Physical Review B**38** (1988) 805–807.
[30] Vinet, P.; Smith, J. R.; Ferrante, J.; Rose, J. H.: Temperature effects on the universal equation of state of solids. Physical Review B**35** (1987) 1945–1953.
[31] Iturbe-Zabalo, E.; Igartua, J. M.; Gateshki, M.: Symmetry-mode analysis of the phase transition in $SrLaZnRuO_6$ and $SrLaMgruO_6$ ordered double perovskites. Journal of Applied Crystallography **46** (2013) 1085–1093.
[32] Wang, Di; Angel, R. J.: Octahedral tilts, symmetry-adapted displacive modes and polyhedral volume ratios in perovskite structures. Acta Crystallographica B**67** (2011) 302–314.
[33] Miller, S. C.; Love, W. F.: Tables of Irreducible Representations of Space Groups and Co-Representations of Magnetic Space Groups. Pruett Press, Boulder (1967).

Received June 4, 2013; accepted November 19, 2013
Published online February 11, 2014